ISSN: 3064-6758 www.aristonpubs.com/sciengg-advances https://doi.org/10.69626/sea.2025.0016

RESEARCH ARTICLE

Electrodeposited MnO_2 Thin Film as High–Performance Electrode for Supercapacitor Application

J. L. Patil [1], R. A. Chavan [1], A. S. Sutar [1], S. S. Kulkarni [1], R. K. Dhanvade [1], P. B. Patil [2], S. R. Shingte[2], S. J. Pawar [1,*]

ABSTRACT: This study presents a facile electrochemical deposition approach for synthesizing MnO_2 thin films directly onto stainless steel (SS) substrates, yielding binder-free nanostructured electrodes for supercapacitor applications. The structural, morphological, and electrochemical characteristics of the deposited MnO_2 films were systematically investigated using X-ray Diffraction (XRD), Fourier Transform Infrared Spectroscopy (FTIR), X-ray Photoelectron Spectroscopy (XPS), and Scanning Electron Microscopy (SEM). XRD analysis confirmed the formation of the amorphous birnessite δ-MnO_2 phase, while FTIR spectra exhibited a characteristic Mn-O stretching vibration at 576 cm^{-1}. XPS spectra indicated the presence of Mn-O-Mn and Mn-O-H bonds, confirming the oxidation states of Mn in the thin film. The electrochemical performance was evaluated using cyclic voltammetry (CV) and galvanostatic charge-discharge (GCD) measurements in a 1M Na_2SO_4 electrolyte. The as-deposited MnO_2 thin film demonstrated a remarkable specific capacitance of 439 F g^{-1} at a current density of 0.5 mA cm^{-2}, along with a power density of 669 W kg^{-1} and an energy density of 61.02 Wh kg^{-1}. The high electrochemical performance of the MnO_2 thin film can be attributed to its nanostructured morphology and amorphous nature, facilitating efficient charge storage. These findings underscore the suitability of electrodeposited MnO_2 as a promising electrode material for next-generation supercapacitors.

Keywords: MnO_2 thin films, Electrodeposition, Supercapacitors, Pseudocapacitance, Energy storage.

Received: 27 July 2024; Revised: 18 September 2024; Accepted: 19 November 2024; Available Online: 08 December 2024

1. INTRODUCTION

The increasing global demand for energy, driven by rapid industrialization and technological advancements, necessitates the development of efficient and sustainable energy storage systems [1, 2]. Among various energy storage technologies, supercapacitors have emerged as promising alternatives to conventional batteries due to their high power density, rapid charge-discharge capability, and long cycle life [3-5]. Unlike traditional batteries that rely on faradaic redox reactions for energy storage, supercapacitors store energy through electrostatic interactions at the electrode-electrolyte interface or through fast reversible surface redox reactions, depending on their classification as electric double-layer capacitors (EDLCs) or pseudocapacitors, respectively [6].

Pseudocapacitors, which utilize transition metal oxides (TMOs) as active electrode materials, have attracted significant interest due to their superior capacitance and energy storage capabilities compared to EDLCs [7, 8]. Among various TMOs, manganese dioxide (MnO_2) is considered a promising electrode material for supercapacitor applications due to its high theoretical capacitance (1370 F g^{-1}), low cost, environmental friendliness, and natural abundance [9-11]. MnO_2 exists in different polymorphic

[1] Shri Vijaysinha Yadav College, Peth Vadgaon, (Affiliated to Shivaji University Kolhapur) Maharashtra, 416112, India.
[2] Department of Physics, The New College, Kolhapur (Affiliated to Shivaji University Kolhapur), Maharashtra, 416012, India.

*Author to whom correspondence should be addressed:
asachinpawar@gmail.com (S. J. Pawar)

forms, including α-, β-, γ-, and δ-MnO_2, each exhibiting unique electrochemical properties [12]. The δ-MnO_2 phase, known as birnessite-type MnO_2, has been reported to exhibit superior electrochemical performance due to its layered structure, which facilitates rapid ion diffusion and intercalation [13].

Despite its advantages, MnO_2 suffers from certain limitations that hinder its practical application in supercapacitors, including poor electrical conductivity (~10^{-5} to 10^{-6} S cm^{-1}) and limited cycling stability due to structural degradation during charge-discharge processes [14, 15]. Various strategies have been explored to overcome these limitations, such as doping with conductive materials (e.g., carbon nanotubes, graphene, or conductive polymers), fabricating nanostructured morphologies, and optimizing the synthesis method to enhance the electrochemical properties of MnO_2-based electrodes [16-18]. Among different fabrication techniques, electrodeposition has emerged as an efficient and scalable approach for synthesizing MnO_2 thin films with controlled thickness, morphology, and porosity [19].

Electrodeposition offers several advantages over conventional synthesis methods, including precise control over film growth, uniform deposition on conductive substrates, and the ability to produce binder-free electrodes [20]. This method enables the formation of nanostructured MnO_2 films directly onto current collectors, eliminating the need for additional binders or conductive additives, which often compromise the overall electrochemical performance of the electrode [21]. Furthermore, the amorphous nature of electrodeposited MnO_2 has been reported to enhance charge storage by providing more active sites for faradaic reactions compared to its crystalline counterparts [22].

Several studies have demonstrated the effectiveness of electrodeposited MnO_2 thin films for supercapacitor applications. For instance, electrodeposited MnO_2 nanostructures have shown specific capacitance values exceeding 400 F g^{-1}, with excellent rate capability and cycling stability [23]. The electrochemical performance of MnO_2 electrodes is significantly influenced by factors such as deposition parameters, film thickness, morphology, and electrolyte composition [24]. In particular, the use of aqueous electrolytes, such as Na_2SO_4, KCl, and Li_2SO_4, has been shown to enhance the capacitive behavior of MnO_2 electrodes by facilitating efficient ion transport and redox reactions [25].

In this study, we report the electrochemical deposition of amorphous MnO_2 thin films onto stainless steel (SS) substrates for supercapacitor applications. The structural, morphological, and electrochemical properties of the as-deposited MnO_2 films were systematically investigated using X-ray Diffraction (XRD), Fourier Transform Infrared Spectroscopy (FTIR), X-ray Photoelectron Spectroscopy (XPS), and Scanning Electron Microscopy (SEM). The electrochemical performance of the MnO_2 electrodes was evaluated using cyclic voltammetry (CV) and galvanostatic charge-discharge (GCD) measurements in a 1 M Na_2SO_4 electrolyte. The results revealed that the electrodeposited MnO_2 thin film exhibited a high specific capacitance of 439 F g^{-1} at a current density of 0.5 mA cm^{-2}, along with a power density of 669 W kg^{-1} and an energy density of 61.02 Wh kg^{-1}. These findings highlight the potential of electrodeposited MnO_2 as a high-performance electrode material for next-generation supercapacitors.

2. EXPERIMENTAL DETAILS

2.1. Materials and Reagents

Analytical-grade sulfuric acid (H_2SO_4) and manganese sulfate ($MnSO_4$) were procured from Loba Chemical Pvt. Ltd. and used without further purification. A 0.2 mm thick commercially available 304-grade stainless steel (SS) substrate was used as the working electrode. All solutions were prepared using double-distilled water (DDW).

2.2. Synthesis Method

The MnO_2 thin film was deposited onto a stainless steel (SS) substrate (1 × 5 cm^2). Initially, the SS substrate was mirror-polished using zero-grade polishing paper, then cleaned with labolene, and subsequently washed with DDW. Finally, it was ultrasonically cleaned for 20 minutes to remove any remaining impurities.

A standard three-electrode setup was employed for the electrochemical deposition, with platinum wire as the counter electrode, an Ag/AgCl electrode as the reference electrode, and SS as the working electrode. The MnO_2 film was cathodically electrodeposited from an aqueous solution containing 0.1 M $MnSO_4$. The pH of the solution was adjusted to 1.0 using H_2SO_4, followed by stirring for 30 minutes to ensure homogeneity. The deposition was carried out at a potential of 2.2 V for 20 minutes, resulting in a dark black MnO_2 film with good adhesion to the substrate. The deposited film was then rinsed with DDW and allowed to air dry for one hour. Figure 1 illustrates the schematic representation of the synthesized MnO_2 thin film.

2.3. Material Characterization

The structural phase of the electrodeposited MnO_2 thin film was analyzed using an X-ray diffractometer (XRD, Rigaku Smart Lab) with Cu-Kα radiation (λ = 1.54 Å). The surface morphology and elemental composition were examined using scanning electron microscopy (SEM, JSM-7800F, JEOL) coupled with energy-dispersive X-ray spectroscopy (EDS; Oxford X-Max). Functional groups present in the MnO_2 thin film were identified through Fourier transform infrared spectroscopy (FTIR; Perkin-Elmer Model No. 100, USA). Additionally, X-ray photoelectron spectroscopy (XPS; Thermo Fisher K-Alpha 250xi) was employed for elemental and chemical state analysis.

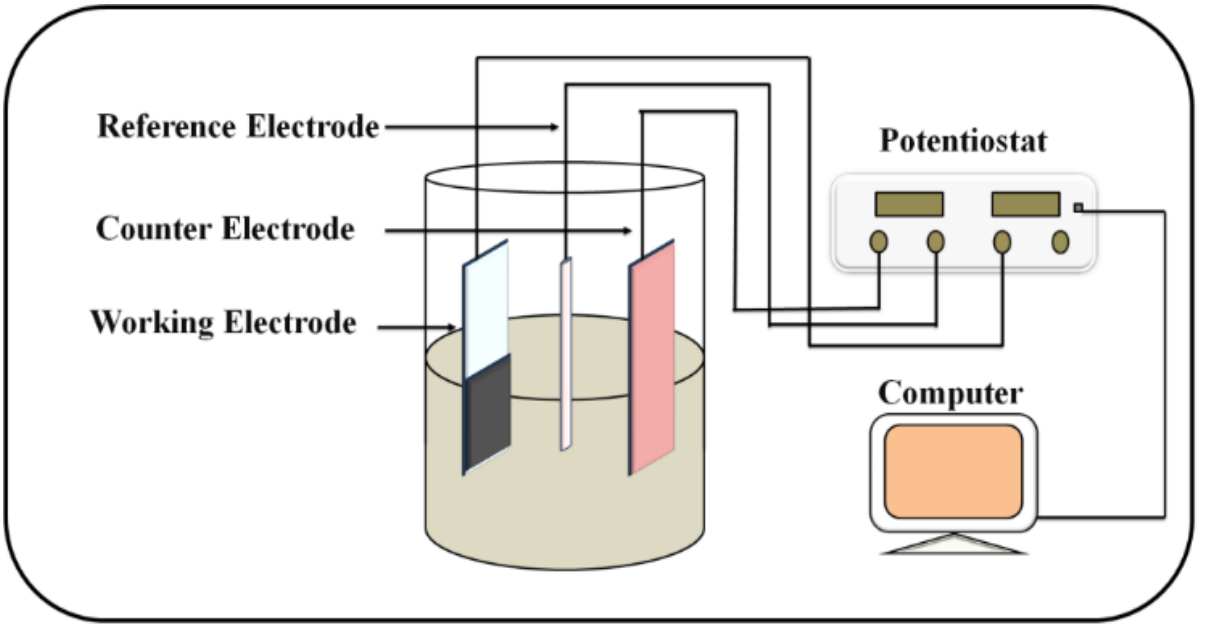

Fig. 1. Schematic of the preparation of MnO_2 electrode.

2.4. Electrochemical Measurements

The electrochemical performance of the MnO_2 thin film was evaluated using a versatile multichannel potentiostat (Princeton Applied Research, VMP2/Z) in a three-electrode configuration. The setup consisted of the as-deposited MnO_2 thin film as the working electrode, an Ag/AgCl electrode as the reference, and platinum wire as the counter electrode, with 1 M Na_2SO_4 serving as the electrolyte. Cyclic voltammetry (CV) and galvanostatic charge-discharge (GCD) measurements were conducted within a potential window of -0.2 V to 0.8 V.

The areal capacitance (C) was calculated from the CV profile using the equation (1):

$$C = \frac{\int_{V_1}^{V_2} I(V)dV}{v(V_2 - V_1)} \quad (1)$$

Where $\int_{V_1}^{V_2} I(V)dV$ represents the area enclosed by the CV curve over a voltage window of ($V_2 - V_1$) at scan rate ν for the film of area 1 x 1 cm^2.

The specific capacitance (C_{SP}) of the MnO_2 thin film was determined from the GCD curves using the following equation [15, 16]:

$$C_{SP} = \frac{I\Delta t}{\Delta V m} \quad (2)$$

where, I is the response current ($mAcm^{-2}$), Δt is the discharge time (s), m is the electrode mass (g) as determined by the weight difference method, ΔV is the potential range (V), and Csp is the specific capacitance (F g^{-1}). Equations (3) and (4) are used to compute the power density (P, W kg^{-1}) and energy density (E, W h kg^{-1}) of the three-electrode based on the GCD curves. In which t(s) is the discharge duration and ΔV (V) is the applied potential window. [5, 17, 18].

$$E = \frac{0.5 C_{SP} (\Delta V)^2}{3.6} \quad (3)$$

$$P = \frac{E \times 3600}{t} \quad (4)$$

Where, t is the discharge duration (s) and ΔV is the applied potential window (V).

3. RESULTS AND DISCUSSION

3.1. Characterization and Properties

XRD analysis was performed on the as-deposited MnO_2 thin films to confirm the formation of MnO_2 and assess its structural characteristics. Figure 2(a) presents the XRD pattern of the MnO_2 thin film deposited on the SS substrate. The diffraction pattern exhibits broad and faint peaks at approximately 12˚, 25˚, and 35˚, which correspond to the (001), (002), and (111) diffraction planes of MnO_2, as indexed according to JCPDS card No. 80-1098. The broad peak nature suggests a low degree of crystallinity, indicative of an amorphous phase. Specifically, the obtained pattern confirms the formation of birnessite-type δ-MnO_2, which is known for its layered structure and excellent electrochemical properties [19-20].

The presence of amorphous δ-MnO_2 is particularly

beneficial for electrochemical applications. The disordered structure and strong non-crystallinity enhance the availability of active sites and promote ion diffusion within the material, leading to improved pseudocapacitive performance [21]. Compared to crystalline MnO_2 phases, which typically have restricted ion transport pathways, amorphous MnO_2 provides higher surface area, improved charge storage capabilities, and faster redox reactions**,** making it a promising candidate for supercapacitor electrodes.

The functional group analysis of the MnO_2 thin film was conducted using Fourier-transform infrared (FTIR) spectroscopy, as shown in Figure 2(b). The spectrum exhibits characteristic absorption bands corresponding to Mn–O stretching vibrations, confirming the presence of MnO_2. The broad absorption band observed around 3400 cm^{-1} is attributed to the O–H stretching vibration of surface hydroxyl groups and adsorbed water molecules. This suggests the presence of hydrated MnO_2, which is beneficial for electrochemical applications due to its ability to enhance ionic conductivity.

Additionally, peaks in the range of 500–800 cm^{-1} correspond to Mn–O vibrations, which are characteristic of MnO_2. The band near 720 cm^{-1} is associated with Mn–O stretching in octahedral coordination, confirming the formation of MnO_2 with a birnessite-like layered structure [22]. The presence of surface hydroxyl groups and adsorbed water molecules further supports the hypothesis that the deposited MnO_2 has an amorphous nature with hydrated characteristics. This structural feature is advantageous for electrochemical energy storage applications, as it promotes efficient ion transport and enhances charge storage capacity.

X-ray photoelectron spectroscopy (XPS) was employed to investigate the oxidation states, surface chemical composition, and binding energies of the as-deposited MnO_2 thin film. This technique provides valuable insights into the electronic structure and chemical bonding of the material, which directly influences its electrochemical properties. Figure 3(a) displays the wide-scan XPS survey spectrum of the MnO_2 thin film, revealing prominent peaks corresponding to manganese (Mn) and oxygen (O) elements. The absence of significant impurity peaks suggests that the deposited MnO_2 is of high purity, further confirming the successful formation of the desired phase.

Figures 3(b) and 3(c) present the high-resolution spectra of Mn 2p and O 1s, respectively, along with the fitted peaks. The Mn 2p spectrum exhibits two well-defined peaks at binding energies of approximately 642.4 eV and 654.1 eV, corresponding to the spin-orbit split levels Mn $2p_{3/2}$ and Mn $2p_{1/2}$, respectively. The energy separation of 11.7 eV between these peaks is characteristic of Mn in the +4 oxidation state (Mn^{4+}), confirming the formation of MnO_2 as the dominant phase [23, 26]. The presence of Mn^{4+} is crucial for enhancing the electrochemical activity of MnO_2-based electrodes, as it facilitates efficient redox reactions in energy storage applications.

The high-resolution O 1s spectrum, shown in Figure 3(c), has been deconvoluted into two distinct peaks, each representing different oxygen environments within the MnO_2 structure. The first peak, located at 529.7 eV, is attributed to lattice oxygen (Mn–O–Mn), which forms the primary MnO_2 framework. This strong Mn–O bond plays a critical role in maintaining the structural stability of MnO_2 and ensuring long-term electrochemical performance. The second peak, appearing at 531.2 eV, corresponds to surface hydroxyl species (Mn–O–H), which arise due to oxygen vacancies or adsorbed hydroxyl groups [24]. The presence of Mn–O–H species suggests a hydrated MnO_2 surface, which can improve ionic conductivity and electrochemical charge storage by facilitating rapid ion diffusion during redox reactions.

To further validate the elemental composition of the MnO_2 thin film, energy-dispersive X-ray spectroscopy (EDS) analysis was performed, as illustrated in Figure 3(d).

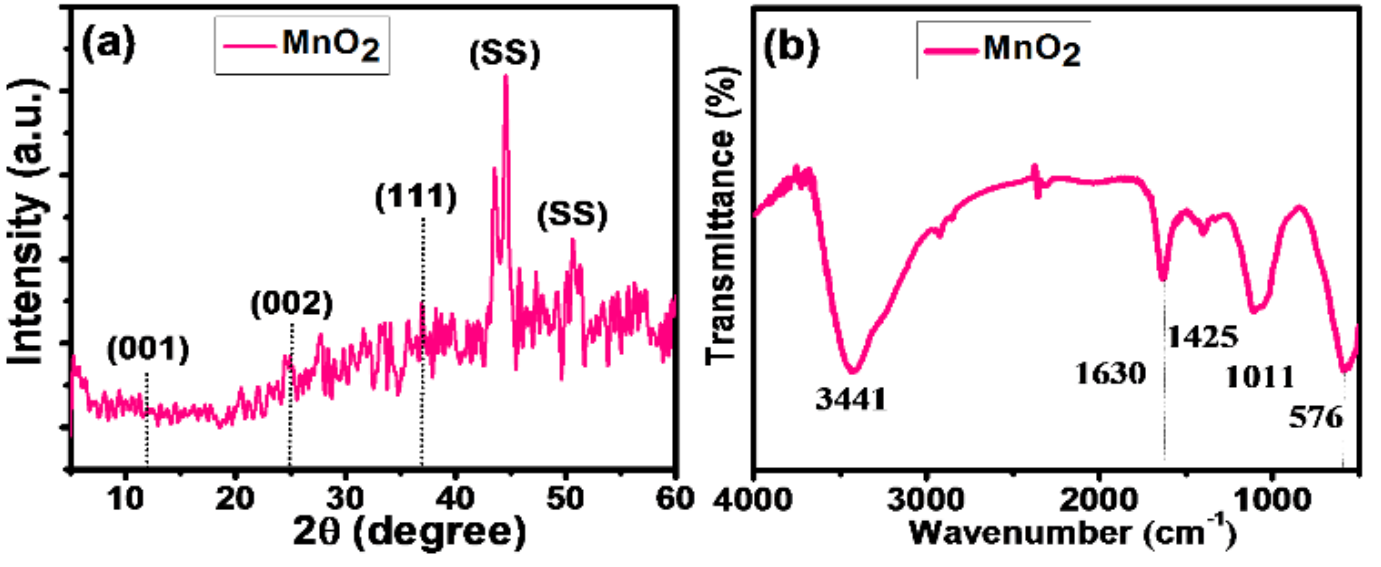

Fig. 2. (a) XRD pattern and (b) FTIR spectrum of MnO_2 thin film.

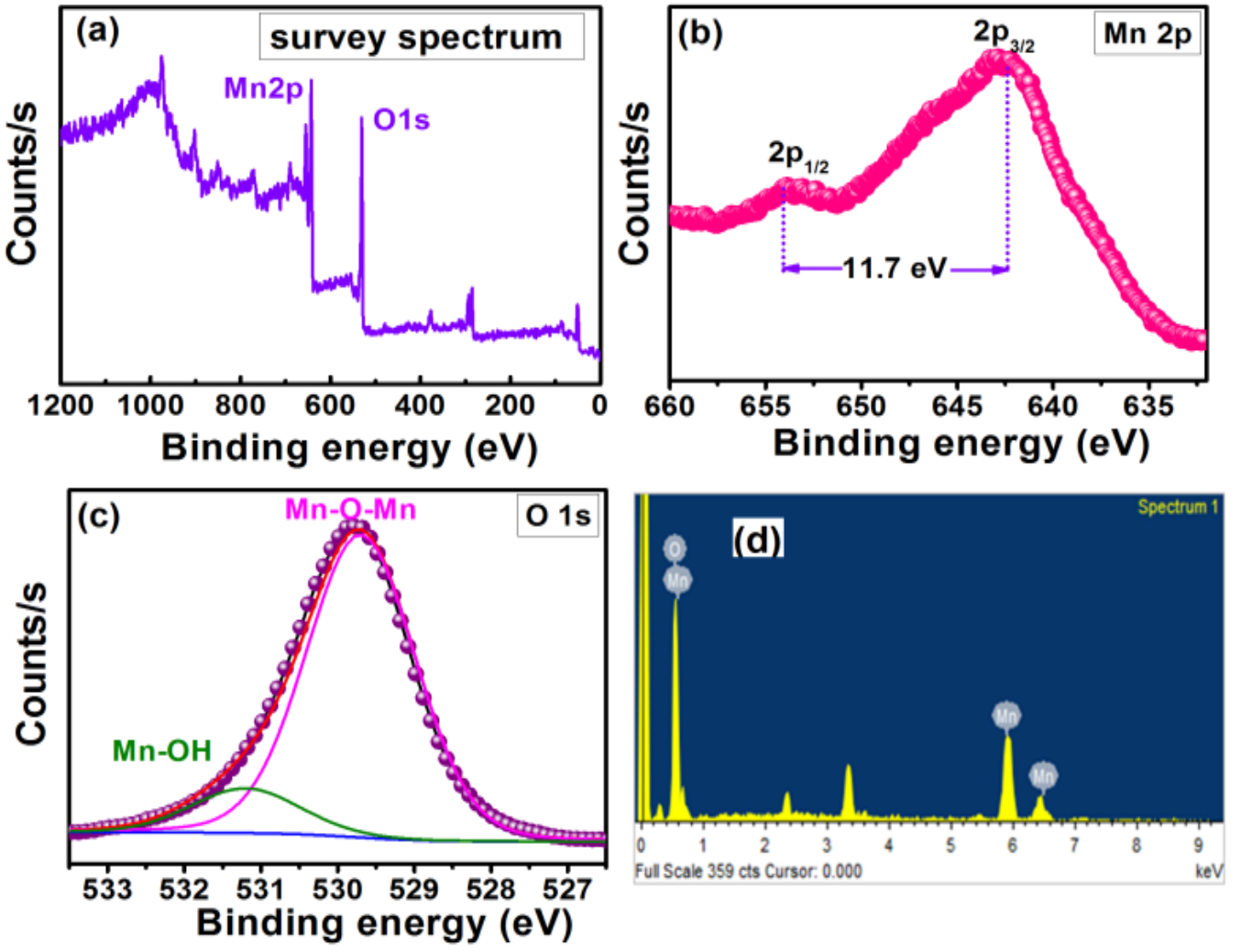

Fig. 3. (a) XPS survey spectrum of MnO_2, The high-resolution XPS spectra of (b) Mn 2p and (c) O 1s, (d) EDX spectrum of MnO_2 thin film.

The EDS spectrum exhibits well-defined peaks corresponding to manganese (Mn) and oxygen (O), with no detectable impurities. This confirms the successful deposition of a high-purity MnO_2 thin film. The atomic ratio of Mn to O, obtained from EDS quantification, is consistent with the expected stoichiometry of MnO_2, further verifying the composition of the material. The XPS and EDS analyses collectively confirm the successful formation of MnO_2 with a dominant Mn^{4+} oxidation state, a well-defined Mn–O–Mn framework, and surface hydroxyl groups that could enhance electrochemical performance.

The surface morphology of the as-deposited MnO_2 thin films was analyzed using scanning electron microscopy (SEM), which provides crucial insights into the material's structural characteristics and potential electrochemical behavior. Figure 4(a) presents a low-magnification SEM image of the MnO_2 thin film, revealing a uniform and continuous surface with densely packed spherical nanoparticles. The homogeneous distribution of these particles suggests a well-controlled deposition process, ensuring structural integrity and uniformity across the film. Such uniformity is essential for achieving consistent electrochemical performance in energy storage applications.

A higher-magnification SEM image, shown in Figure 4(b), provides a closer look at the individual MnO_2 particles. The image clearly depicts a distinct spherical morphology, resembling that of a spongy ball. This unique nanostructured surface, characterized by a high degree of porosity and interparticle connectivity, plays a crucial role in enhancing the electrochemical properties of MnO_2 thin films. The nanoscale spherical architecture increases the surface-area-to-volume ratio, thereby offering a larger number of electroactive sites for faradaic reactions. This, in turn, facilitates rapid charge storage and improved capacitive behavior.

Furthermore, the observed spongy and pliable morphology is expected to enhance ion and electron transport within the MnO_2 matrix. The interconnected porous structure enables better penetration of electrolyte ions into the active material, ensuring efficient ionic diffusion pathways.

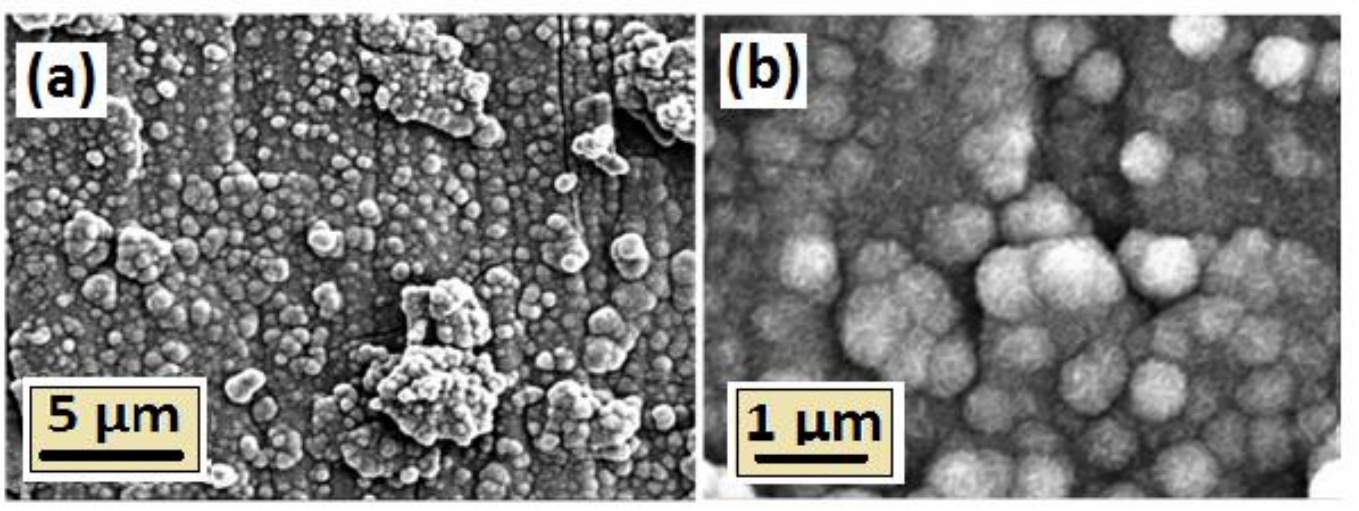

Fig. 4. Low (a) and high (b) magnification images of MnO_2 thin film.

Additionally, the nanospherical MnO_2 particles provide a conductive framework that minimizes charge-transfer resistance and promotes faster electron mobility. These characteristics contribute significantly to the overall electrochemical performance, making the MnO_2 thin films highly suitable for applications in supercapacitors and other energy storage devices. The SEM analysis confirms the successful deposition of MnO_2 thin films with a well-defined nanostructure, which can play a pivotal role in optimizing their electrochemical efficiency. The combination of a uniform, porous, and spherical morphology provides a strong foundation for further investigations into the material's charge storage mechanisms and practical applicability in energy-related technologies.

3.2. Supercapacitor application of MnO_2 thin films

The MnO_2 thin film electrode was tested electrochemically as it was deposited. The CV profiles depicted in Figure 5(a) display the correlation between different potential scans (5 to 100 mV s^{-1}) within active potential window of -0.2 to 0.8 V (vs Ag/AgCl). The finding of a quasi-rectangular CV shape with a wide redox shoulder indicates that faradic processes mostly control capacitance. This phenomenon arises from electrochemical reactions associated with Mn/Mnn+. Furthermore, the observed rise in peak current proportionate to the scan rates ranging from 5 to100 mVs^{-1} indicates a favourable pseudo-enriched capacitive storage of the electrode. Furthermore, increasing the scan rate to 100 mV s^{-1} does not result in any noticeable change in the cyclic voltammetry profile, demonstrating good electrochemical reversibility and the ability for rapid charge-discharge. Increased scan rates decrease the duration of interaction between electrolyte ions and the nanostructured electrode, resulting in a decrease in capacitance [25, 26].

The MnO_2 thin film sample was subjected to GCD analysis at distinct current densities spanning from 0.5 to 3.0 mA cm^{-2} within active potential window -0.2 to 0.8 V. The GCD profile is shown in Figure 5(b), which exhibits an irregular triangular shape across all current densities, is consistent with the redox waves observed in the corresponding CV curves. This is a characteristic of faradic pseudocapacitance. The non-linear GCD profile of the MnO_2 electrode exhibits a distinctive shape, which can be further categorized into three types: (i) At the onset of discharging, a minimal internal resistance component results in a negligible voltage drop (iR). (ii) A nearly linear shift within the potential range indicates excellent reversibility of the electrode. (iii) The ramp-like portion indicates efficient faradic activity resulting from redox interactions between the active material and electrolyte. Based on CV, the areal capacitance obtained were 21.2, 17.4, 13.2, 9.6, 7.9, 6.8, and 5.6 mF cm^{-1} at scan rate of 5, 10, 20, 40, 60, 80, and 100 mV s^{-1}. The electrode demonstrates specific capacitance of 439, 242, 181, and 90 F g^{-1} at 0.5, 1, 2, and 3 mA cm^{-2} respectively. As illustrated in Figure 5(c), the specific capacitance decreased as the current density increased because the electrode did not have enough time to interact with the electrolyte. The highest capacitance obtained is 439 F g^{-1} at 0.5 mA cm^{-2}. The strong non-crystallinities found in as-deposited amorphous MnO_2 will facilitate the creation of large active regions, leading to increased pseudocapacitive performance. Similar behaviour was identified by Nikamet al. who obtained improved supercapacitive properties for amorphous cobalt ferrite thin film deposited at room temperature by pulsed laser deposition method [26]. The calculated power densities were 669, 1499, 3134, and 5824 W kg^{-1}, at energy densities of 61.02, 33.66, 25.25, and 12.62 W h kg^{-1}. The MnO_2 electrode demonstrates a peak power density of 669 W kg^{-1} and an energy density of 61.02 W h kg-1 at 0.5 mA cm^{-2}. Furthermore, a peak areal capacitance of 21.2 mF cm^{-1} was achieved at a scan rate of 5 mV s^{-1}, as shown in Figure 5(d).

Electrochemical Impedance Spectroscopy (EIS) was utilized to investigate the ion transport behavior and charge storage dynamics of the MnO_2 thin film electrode in a 1 M

Na_2SO_4 electrolyte solution. The EIS measurements were conducted over a broad frequency range, spanning from 1000 kHz to 1 Hz, with an applied AC perturbation of 5 mV. This technique provides valuable insights into the resistive and capacitive properties of the electrode, which are crucial for evaluating its electrochemical performance. Figure 6(a) presents the Nyquist plot, which consists of a semicircle in the high-frequency region and a linear tail in the low-frequency region. The appearance of a small semicircle at high frequencies is indicative of charge transfer resistance (R_{ct}), while the linear segment at lower frequencies corresponds to the ion diffusion behavior of the electrolyte within the electrode material.

The equivalent series resistance (RESR), which accounts for the combined resistance of the electrolyte, the intrinsic resistance of the electrode material, the current collector, and the electrode/current collector interface, was found to be 4.1 Ω. A low RESR value suggests efficient charge transport and minimal ohmic losses, which are desirable characteristics for high-performance energy storage devices. The charge transfer resistance (R_{ct}), determined from the semicircle diameter in the high-frequency region, was measured at 2.4 Ω. This relatively low R_ct value indicates a facile charge transfer process between the MnO_2 electrode and the electrolyte, which is crucial for enhancing the electrochemical reaction kinetics. The efficient electron and ion transport at the electrode-electrolyte interface contributes to the rapid redox reactions associated with pseudocapacitive charge storage.

Furthermore, the phase angle of the MnO_2 thin film was observed to be 54.9°, confirming its pseudocapacitive behavior (Figure 6 (b)). This result is consistent with the findings from Cyclic Voltammetry (CV) and Galvanostatic Charge-Discharge (GCD) measurements, which also indicate that the MnO_2 thin film operates through a faradaic charge storage mechanism.

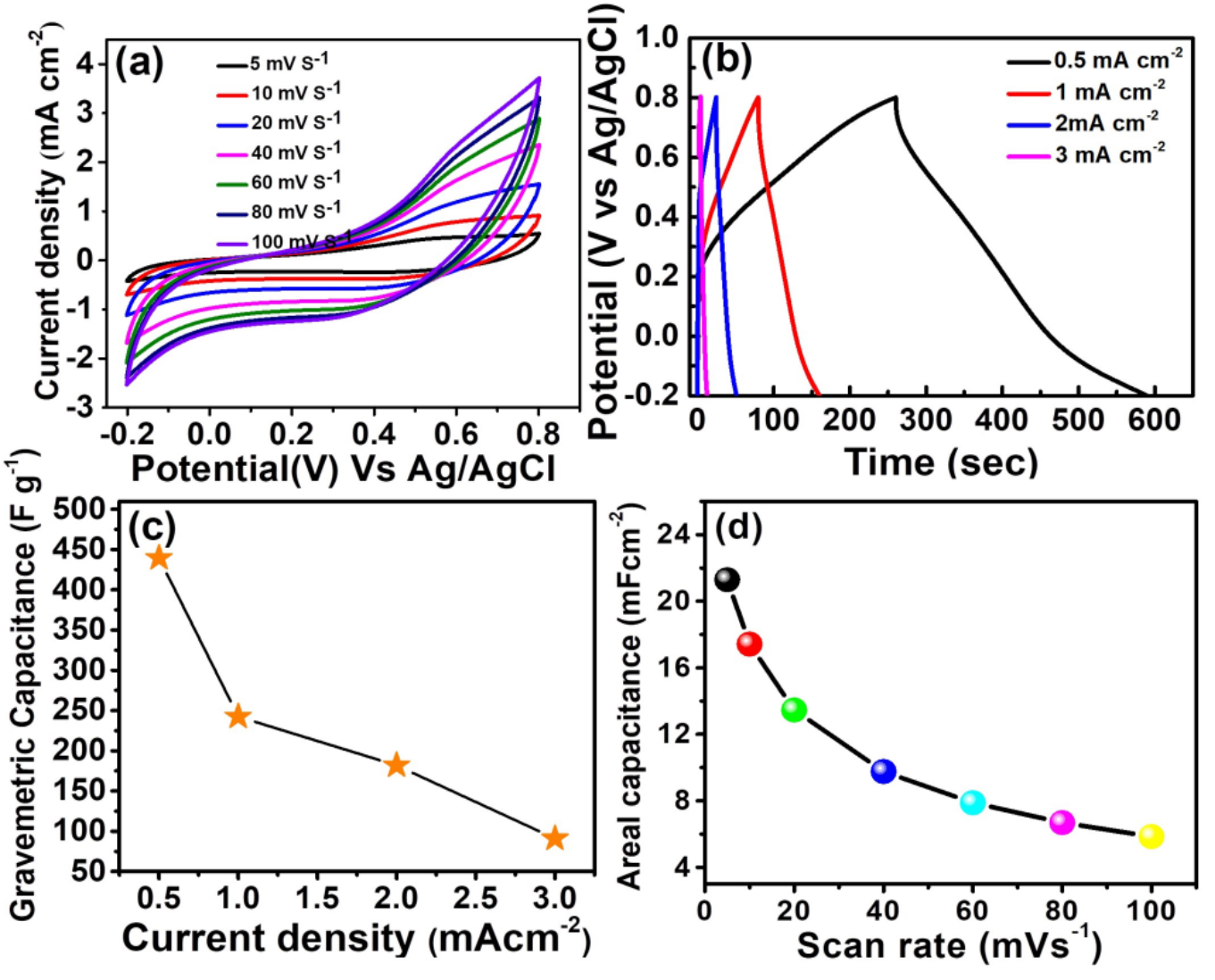

Fig. 5. (a) CV, (b) GCD responses of MnO_2, Plots of (c) specific capacitance response with current density and (d) areal capacitance v/s scan rate.

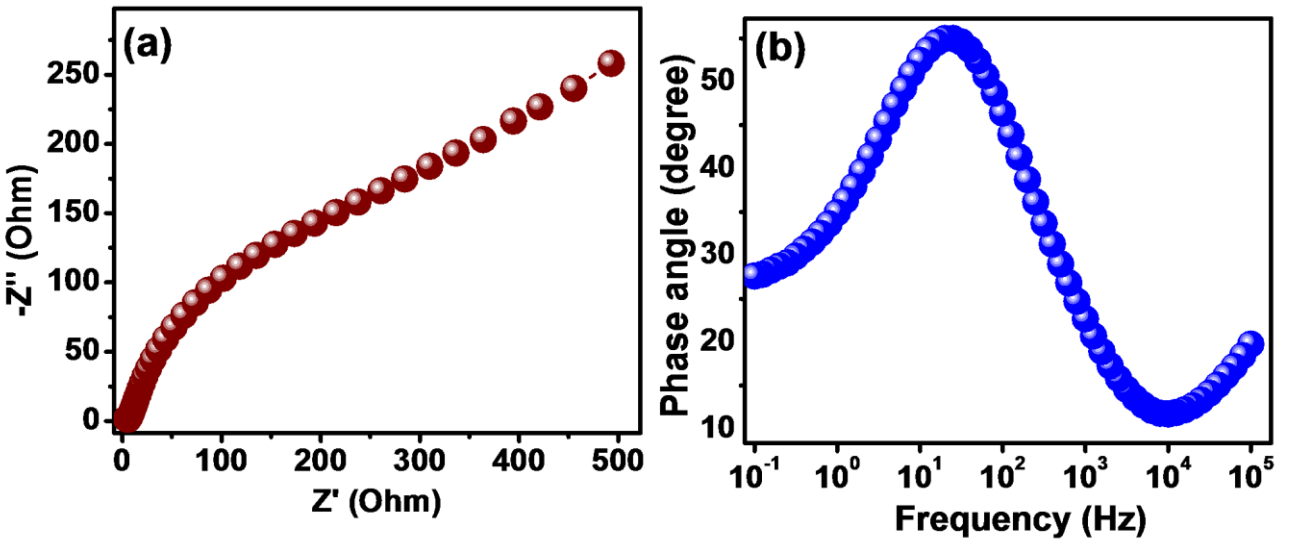

Fig. 6. (a) Nyquist plot (b) Bodes plot of MnO_2 thin film.

The deviation of the phase angle from the ideal capacitive value of 90° suggests a combination of capacitive and resistive characteristics, a typical feature of pseudocapacitive materials. The EIS analysis reveals that the MnO_2 thin film exhibits low internal resistance, efficient charge transport, and pseudocapacitive characteristics, making it a promising electrode material for high-performance supercapacitors. The observed electrochemical properties demonstrate that the electrode material can facilitate rapid charge-discharge cycles, which is essential for practical energy storage applications.

4. CONCLUSION

In this study, MnO_2 thin films were successfully electrodeposited onto stainless steel substrates using a simple and cost-effective electrochemical approach, resulting in binder-free nanostructured electrodes for supercapacitor applications. The structural and compositional analyses confirmed the amorphous nature of the deposited MnO_2, with XRD revealing the birnessite δ-MnO_2 phase and FTIR and XPS analyses providing insights into its bonding characteristics. SEM imaging demonstrated the formation of a uniform and porous morphology, which is beneficial for ion diffusion and charge storage. Electrochemical investigations using cyclic voltammetry and galvanostatic charge-discharge techniques demonstrated superior capacitive behavior of the MnO_2 thin film, with a high specific capacitance of 439 F g^{-1} at a current density of 0.5 mA cm^{-2}. The electrode exhibited an impressive power density of 669 W kg^{-1} and an energy density of 61.02 Wh kg^{-1}, signifying its potential for high-performance energy storage applications. The observed electrochemical properties suggest that the amorphous nature of MnO_2 enhances the accessibility of active sites, leading to improved charge storage capabilities. Compared to conventional electrode fabrication methods, the electrochemical deposition technique employed in this work offers several advantages, including uniform film formation, cost-effectiveness, and environmental sustainability. The binder-free nature of the MnO_2 thin film further enhances its practical applicability in supercapacitors by eliminating the need for additional conductive additives or binders, which often reduce electrochemical efficiency. The results highlight the potential of electrodeposited MnO_2 thin films as promising candidates for next-generation supercapacitors. Future research could focus on optimizing deposition parameters, exploring hybrid MnO_2-based composites, and evaluating long-term cycling stability to further enhance the performance of these electrode materials. This study provides a foundation for the development of efficient, scalable, and sustainable energy storage solutions.

DECLARATIONS

Ethical Approval

We affirm that this manuscript is an original work, has not been previously published, and is not currently under consideration for publication in any other journal or conference proceedings. All authors have reviewed and approved the manuscript, and the order of authorship has been mutually agreed upon.

Funding

Not applicable

Availability of data and material

All of the data obtained or analyzed during this study is included in the report that was submitted.

Conflicts of Interest

The authors declare that they have no financial or personal interests that could have influenced the research and findings presented in this paper. The authors alone are responsible for the content and writing of this article.

Authors' contributions

All authors contributed equally in the preparation of this manuscript.

ACKNOWLEDGEMENTS

One of the authors, Dr. Sachin Pawar acknowledges financial support from Shivaji University Kolhapur under the "Research Sensitization Scheme for College Students of Lead College Scheme".

REFERENCES

[1] Arif, M., Sanger, A. and Singh, A., **2018.** Sputter deposited chromium nitride thin electrodes for supercapacitor applications. *Materials Letters*, *220*, pp.213-217. https://doi.org/10.1016/j.matlet.2018.02.094.

[2] Heubner, C., Nikolowski, K., Reuber, S., Schneider, M., Wolter, M. and Michaelis, A., **2021.** Recent insights into rate performance limitations of Li-ion batteries. *Batteries & Supercaps*, *4*(2), pp.268-285. https://doi.org/10.1002/batt.202000227.

[3] Kraytsberg, A. and Ein-Eli, Y., **2011.** Review on Li–air batteries—Opportunities, limitations and perspective. *Journal of Power Sources*, *196*(3), pp.886-893. https://doi.org/10.1016/j.jpowsour.2010.09.031

[4] Liang, Y., Zhao, C.Z., Yuan, H., Chen, Y., Zhang, W., Huang, J.Q., Yu, D., Liu, Y., Titirici, M.M., Chueh, Y.L. and Yu, H., **2019.** A review of rechargeable batteries for portable electronic devices. *InfoMat*, *1*(1), pp.6-32. https://doi.org/10.1002/inf2.12000.

[5] Chavan, R.A., Kamble, G.P., Dhavale, S.B., Rasal, A.S., Kolekar, S.S., Chang, J.Y. and Ghule, A.V., **2023.** NiO@ MXene nanocomposite as an anode with enhanced energy density for asymmetric supercapacitors. *Energy & Fuels*, *37*(6), pp.4658-4670. https://doi.org/10.1021/acs.energyfuels.2c04206

[6] Vadiyar, M.M., Bhise, S.C., Kolekar, S.S., Chang, J.Y., Ghule, K.S. and Ghule, A.V**., 2016.** Low cost flexible 3-D aligned and cross-linked efficient $ZnFe_2O_4$ nano-flakes electrode on stainless steel mesh for asymmetric supercapacitors. *Journal of Materials Chemistry A*, *4*(9), pp.3504-3512. https://doi.org/10.1039/C5TA09022A.

[7] Simon, P. and Gogotsi, Y., **2008.** Materials for electrochemical capacitors. *Nature materials*, *7*(11), pp.845-854. https://doi.org/10.1038/nmat2297.

[8] Yang, H.Z. and Zou, J.P., **2018.** Controllable preparation of hierarchical NiO hollow microspheres with high pseudo-capacitance. *Transactions of Nonferrous Metals Society of China*, *28*(9), pp.1808-1818. https://doi.org/10.1016/S1003-6326(18)64825-3

[9] Bi, R.R., Wu, X.L., Cao, F.F., Jiang, L.Y., Guo, Y.G. and Wan, L.J., **2010.** Highly dispersed RuO_2 nanoparticles on carbon nanotubes: facile synthesis and enhanced supercapacitance performance. *The Journal of Physical Chemistry C*, *114*(6), pp.2448-2451. https://doi.org/10.1021/jp9116563

[10] Eskusson, J., Rauwel, P., Nerut, J. and Jänes, A., **2016.** A hybrid capacitor based on Fe_3O_4-graphene nanocomposite/few-layer graphene in different aqueous electrolytes. *Journal of The Electrochemical Society*, *163*(13), p.A2768. DOI:10.1149/2.1161613jes.

[11] Wang, M., Cheng, S., Dang, G., Min, F., Li, H., Zhang, Q. and Xie, J., **2017.** Solvothermal synthesized γ-Fe_2O_3/graphite composite for supercapacitor. *International Journal of Electrochemical Science*, *12*(7), pp.6292-6303. https://doi.org/10.20964/2017.07.75.

[12] Kashale, A.A., Vadiyar, M.M., Kolekar, S.S., Sathe, B.R., Chang, J.Y., Dhakal, H.N. and Ghule, A.V., **2017.** Binder free 2D aligned efficient MnO_2 micro flowers as stable electrodes for symmetric supercapacitor applications. *RSC Advances*, *7*(59), pp.36886-36894. https://doi.org/10.1039/C7RA05655A.

[13] Wang, H., Ren, Q., Brett, D.J., He, G., Wang, R., Key, J. and Ji, S., **2017**. Double-shelled tremella-like NiO@ Co_3O_4@ MnO_2 as a high-performance cathode material for alkaline supercapacitors. *Journal of Power Sources*, *343*, pp.76-82. https://doi.org/10.1016/j.jpowsour.2017.01.042.

[14] Parveen, N. and Ansari, S.A., **2024.** Fabrication and Characterization of High-Capacity Manganese Oxide Based Supercapacitor Electrode. *ChemSci Advances*, *1*(1), pp.41-46. https://doi.org/10.69626/csa.2024.0041

[15] Zhang, J., Guo, C., Zhang, L. and Li, C.M., **2013**. Direct growth of flower-like manganese oxide on reduced graphene oxide towards efficient oxygen reduction reaction. *Chemical Communications*, *49*(56), pp.6334-6336. https://doi.org/10.1039/C3CC42127A.

[16] Kamble, G.P., Rasal, A.S., Gaikwad, S.B., Gurav, V.S., Chang, J.Y., Kolekar, S.S., Ling, Y.C. and Ghule, A.V., **2021.** $CuCo_2O_4$ nanorods coated with CuO nanoneedles for supercapacitor applications. *ACS Applied Nano Materials*, *4*(11), pp.12702-12711.

https://doi.org/10.1021/acsanm.1c03284.

[17] Kamble, G.P., Kashale, A.A., Rasal, A.S., Mane, S.A., Chavan, R.A., Chang, J.Y., Ling, Y.C., Kolekar, S.S. and Ghule, A.V., **2021.** Marigold micro-flower like $NiCo_2O_4$ grown on flexible stainless-steel mesh as an electrode for supercapacitors. *RSC advances*, *11*(6), pp.3666-3672. https://doi.org/10.1039/D0RA09524A

[18] Patil, P.D., Shingte, S.R., Karade, V.C., Kim, J.H., Dongale, T.D., Mujawar, S.H., Patil, A.M. and Patil, P.B., **2021.** Effect of annealing temperature on morphologies of metal organic framework derived $NiFe_2O_4$ for supercapacitor application. *Journal of Energy Storage*, *40*, p.102821. https://doi.org/10.1016/j.est.2021.102821.

[19] Chen, R., Yu, J. and Xiao, W., **2013.** Hierarchically porous MnO_2 microspheres with enhanced adsorption performance. *Journal of Materials Chemistry A*, *1*(38), pp.11682-11690. https://doi.org/10.1039/C3TA12589K.

[20] Huang, M., Zhang, Y., Li, F., Wang, Z., Alamusi, Hu, N., Wen, Z. and Liu, Q., **2014.** Merging of Kirkendall growth and Ostwald ripening: CuO@ MnO_2 core-shell architectures for asymmetric supercapacitors. *Scientific Reports*, *4*(1), p.4518. https://doi.org/10.1038/srep04518.

[21] Bai, H., Liang, S., Wei, T., Zhou, Q., Shi, M., Jiang, Z., Feng, J., Zhang, M. and Fan, Z., **2022.** Enhanced pseudo-capacitance and rate performance of amorphous MnO_2 for supercapacitor by high Na doping and structural water content. *Journal of Power Sources*, *523*, p.231032. https://doi.org/10.1016/j.jpowsour.2022.231032.

[22] Ganeshan, S., Ramasundari, P., Elangovan, A., Arivazhagan, G. and Vijayalakshmi, R., **2017.** Synthesis and characterization of MnO_2 nanoparticles: study of structural and optical properties. *International Journal of Scientific Research in Physics and Applied Sciences*, *5*(6), pp.5-8. https://doi.org/10.26438/ijsrpas/v5i6.58.

[23] Audi, A.A. and Sherwood, P.M., **2002**. Valence-band x-ray photoelectron spectroscopic studies of manganese and its oxides interpreted by cluster and band structure calculations. *Surface and Interface Analysis. 33*(3), pp.274-282. https://doi.org/10.1002/sia.1211.

[24] Zhou, J., Yu, J., Shi, L., Wang, Z., Liu, H., Yang, B., Li, C., Zhu, C. and Xu, J., **2018.** A conductive and highly deformable all-pseudocapacitive composite paper as supercapacitor electrode with improved areal and volumetric capacitance. *Small*, *14*(51), p.1803786. https://doi.org/10.1002/smll.201803786.

[25] Jaganyi, D., Altaf, M. and Wekesa, I., **2013.** Synthesis and characterization of whisker-shaped MnO_2 nanostructure at room temperature. *Applied Nanoscience*, *3*, pp.329-333. https://doi.org/10.1007/s13204-012-0135-3.

[26] Nikam, S.M., Sharma, A., Rahaman, M., Teli, A.M., Mujawar, S.H., Zahn, D.R.T., Patil, P.S., Sahoo, S.C., Salvan, G. and Patil, P.B., 2**020.** Pulsed laser deposited $CoFe_2O_4$ thin films as supercapacitor electrodes. *RSC Advances*, *10*(33), pp.19353-19359. DOI: 10.1039/D0RA02564J.

